RESEARCH ARTICLE

Altered basal ganglia infraslow oscillation and resting functional connectivity in complex regional pain syndrome

Barbara Lee[1] | Flavia Di Pietro[2,3] | Luke A. Henderson[1] | Paul J. Austin[1]

[1]School of Medical Sciences and Brain and Mind Centre, University of Sydney, Camperdown, New South Wales, Australia

[2]Curtin Medical School, Faculty of Health Sciences, Curtin University, Bentley, Western Australia, Australia

[3]Curtin Health Innovation Research Institute, Curtin University, Bentley, Western Australia, Australia

Correspondence
Paul J. Austin, School of Medical Sciences, Faculty of Medicine and Health, Brain and Mind Centre, University of Sydney, 94 Mallett Street, Camperdown, NSW 2050, Australia.
Email: paul.austin@sydney.edu.au

Abstract

Complex regional pain syndrome (CRPS) is a painful condition commonly accompanied by movement disturbances and often affects the upper limbs. The basal ganglia motor loop is central to movement, however, non-motor basal ganglia loops are involved in pain, sensory integration, visual processing, cognition, and emotion. Systematic evaluation of each basal ganglia functional loop and its relation to motor and non-motor disturbances in CRPS has not been investigated. We recruited 15 upper limb CRPS and 45 matched healthy control subjects. Using functional magnetic resonance imaging, infraslow oscillations (ISO) and resting-state functional connectivity in motor and non-motor basal ganglia loops were investigated using putamen and caudate seeds. Compared to controls, CRPS subjects displayed increased ISO power in the putamen contralateral to the CRPS affected limb, specifically, in contralateral putamen areas representing the supplementary motor area hand, motor hand, and motor tongue. Furthermore, compared to controls, CRPS subjects displayed increased resting connectivity between these putaminal areas as well as from the caudate body to cortical areas such as the primary motor cortex, supplementary and cingulate motor areas, parietal association areas, and the orbitofrontal cortex. These findings demonstrate changes in basal ganglia loop function in CRPS subjects and may underpin motor disturbances of CRPS.

KEYWORDS
basal ganglia, chronic pain, complex regional pain syndrome, infraslow oscillations, motor dysfunction, putamen, resting-state fMRI

1 | INTRODUCTION

Complex regional pain syndrome (CRPS) is a chronic pain disorder of the limbs, most often affecting the upper limbs (Marinus et al., 2011). The development of CRPS is usually precipitated by an injury such as a fracture but can also occur spontaneously and is characterized by pain, sensory disturbances, motor dysfunction, and autonomic dysregulation (Harden et al., 2007;

Marinus et al., 2011). Motor dysfunction in CRPS can involve a decreased range of motion, muscle weakness, tremor, and dystonia (Harden et al., 2007). Symptoms of CRPS can persist for many years, and the most persistent sign is motor dysfunction (Bean et al., 2014).

To date, cortical circuits have been the primary focus of studies examining motor dysfunction in CRPS, with functional magnetic resonance imaging (fMRI) studies showing altered activation

Edited by Cristina Antonella Ghiani and Nathalie Dehorter.

patterns in the primary motor cortex (M1) and supplementary motor area (SMA) during finger tapping or action observation (Hotta et al., 2017; Maihöfner et al., 2007). Subcortical structures, such as the basal ganglia, are also crucial in motor function, including action selection and voluntary movement (Alexander et al., 1986; Redgrave et al., 2011). Basal ganglia motor loops, via the putamen, are somatotopically organized (Nambu et al., 2002), with thalamocortical projections determining whether a movement in a particular body region is facilitated or suppressed (Albin et al., 1989). It is well established that basal ganglia pathology results in movement disorders (e.g., Parkinson's disease), and specific putamen lesions can lead to dystonia (Neychev et al., 2011), as well as changes in pain perception (Borsook et al., 2010; Starr et al., 2011).

Altered thalamocortical rhythm is associated with neuropathic pain and burst firing of infraslow oscillations (ISOs) (Gerke et al., 2003; Iwata et al., 2011; Sarnthein et al., 2006). In a recent series of studies, we reported differences in resting infraslow oscillations (ISOs) in pain processing regions in individuals with CRPS and other chronic neuropathic pain conditions (Alshelh et al., 2016; Di Pietro et al., 2020). We suggested that these differences may underpin altered thalamocortical rhythm and ultimately in the persistence of pain. Altered thalamocortical rhythm has not only been reported in neuropathic pain. Putamen projections mediate thalamocortical rhythm regulating movement (Opri et al., 2019) and altered thalamocortical rhythm is also found in Parkinson's disease (Vanneste et al., 2018). Furthermore, in Parkinson's disease, increased ISO power is associated with increased motor dysfunction (Hou et al., 2014; Wang et al., 2020). Interestingly, in CRPS subjects, we also found increased ISOs in the region of the putamen with extension into the insula cortex contralateral to the affected limb (Di Pietro et al., 2020). The frequency range of ISO increase in CRPS as well as Parkinson's disease is indicative of astrogliosis as it coincides with the range of astrocytic calcium waves (0.03–0.06 Hz) and release of gliotransmitters (Crunelli et al., 2002; Henderson & Di Pietro, 2016). Indeed, increased ISO and increased astrocyte activation have been found in the same brain regions in neuropathic pain (Alshelh et al., 2016; Okada-Ogawa et al., 2009). Furthermore, optimal astrocytic calcium levels are needed as either attenuating or elevating astrocytic calcium levels lead to motor impairments (Agulhon et al., 2013; Padmashri et al., 2015). Thus, a detailed investigation of ISOs in multiple putamen and caudate seeds in CRPS may reveal underlying astrocytic calcium differences compared to controls that may be related to altered motor function.

Several studies have reported structural and functional connectivity changes in the putamen in adult and pediatric cases of CRPS (Azqueta-Gavaldon et al., 2020; Becerra et al., 2014; Linnman et al., 2013), however, these studies did not evaluate the putamen's somatotopic organization. In addition, functional connectivity changes in non-motor cortico-basal ganglia re-entrant loops that regulate cognition, reward/motivation, visual processing, and sensory integration (Alexander et al., 1986; Choi et al., 2012; Da Cunha et al., 2012; Middleton & Strick, 1996; Redgrave et al., 2010) have been reported in CRPS (Becerra et al., 2014; Geha et al., 2008; Lebel

Significance

Complex regional pain syndrome is a chronic pain disorder affecting the limbs and is associated with motor dysfunction. The basal ganglia are critical in regulating movement but also non-motor functions such as sensory integration, visual processing, and cognition. No previous study has systematically evaluated the functional connectivity of basal ganglia motor and non-motor territories in CRPS. We found that CRPS participants have greater connectivity in cortico-basal ganglia loops specific to motor function and visuospatial integration. Changes in basal ganglia connectivity in CRPS likely underlie motor disturbances like dystonia and tremor and altered visuospatial perception of the CRPS affected limb.

et al., 2008). However, again, these studies did not systematically evaluate each basal ganglia functional loop, nor did they determine if changes were related to sensory, motor, or non-motor disturbances.

The aim of this resting-state fMRI study was to systematically investigate if adult CRPS subjects have altered ISOs and functional connectivity in motor (putamen) and non-motor basal ganglia loops, compared to pain-free control subjects. We hypothesized that CRPS subjects would have altered basal ganglia ISOs and connectivity, and that changes in motor loop activity and connectivity would be associated with motor dysfunction of CRPS.

2 | MATERIALS AND METHODS

This study was approved by the Human Research Ethics Committee of the University of Sydney (HREC reference number 2018/073) and was conducted in accordance with the Declaration of Helsinki. Due to the uncommon nature of CRPS and difficulty in recruiting eligible and willing upper limb CRPS participants, no sample size calculation was performed, hence the study recruited a convenience sample. Prior to study participation, informed written consent was obtained from all participants. Data from the CRPS participants and a subset of the pain-free healthy control participants have been published in prior studies (Di Pietro et al., 2020; Lee et al., 2020).

2.1 | Study participants

Sixteen eligible individuals with CRPS gave consent to participate in the study. Imaging data were not obtained from one CRPS subject due to claustrophobia in the MRI scanner. Thus, imaging data from 15 upper limb CRPS subjects (11 females; mean ± SEM age: 47.5 ± 3.2 years) and 45 age- and sex-matched pain-free healthy controls (33 females; 47.3 ± 1.9 years) were collected. CRPS subjects were diagnosed following the International Association for the Study

of Pain "Budapest" diagnostic criteria (Harden et al., 2007) and had ongoing pain for at least 3 months. CRPS subjects were eligible for the study if they reported other regions of pain or CRPS, but upper limb CRPS was required to be their primary complaint. Exclusion criteria included any MRI contraindications such as cardiac pacemakers and metal implants, or any significant mental health disorders, developmental delays, or neurological disorders that would prevent safe participation.

2.2 | CRPS assessment

The researcher assessed CRPS signs in both upper limbs of each CRPS subject. (i) *Sensory*: Hyperalgesia and allodynia were assessed by pinprick on the dorsal webspace of the hand and light brush strokes on the dorsum of the hands, respectively. (ii) *Vasomotor*: Skin temperature asymmetry was assessed through touch, and skin color changes/asymmetry was assessed visually. (iii) *Sudomotor/edema*: Sweating (sudomotor) was assessed by touching the subject's palms of both hands. Edema was assessed through measurement of the circumference of the wrist and proximal phalanx of the middle finger with a tape measure. Signs of sudomotor function and edema were recorded as present if there was asymmetry between the upper limbs. (iv) *Motor/Trophic*: We observed for motor signs such as tremor and dystonia. Motor weakness was assessed through a power grip test on the researcher's index and middle fingers. Hair, nail, and skin changes/asymmetry between the upper limbs (trophic changes) were assessed visually.

2.3 | Questionnaires

2.3.1 | Each CRPS subject completed several questionnaires

Pain
CRPS participants rated their pain intensity on the day of the study ("day pain") on a 10 cm visual analogue scale (VAS) (0 = no pain to 10 = worst imaginable pain). Using the 10 cm VAS, CRPS subjects were also asked to record their ongoing pain intensity three times a day for 7 days before or following the scanning session. The mean "diary pain" score was obtained by averaging the 21 pain intensity scores.

Functional assessment
The patient-rated Wrist and Hand Evaluation (PRWHE) assessed task-associated pain intensity and functional difficulty of the CRPS affected limb (MacDermid, 1996). The PRWHE is divided into pain and function subscores, as well as total score. The PRWHE pain score ranges from 0 to 50, the function score 0 to 50, and the total score 0 to 100. Higher scores indicate more pain and functional disability of the CRPS affected limb. The shortened 11-item Disabilities of the Arm, Shoulder and Hand (QuickDASH) Outcome Measure

(Beaton et al., 2005) assessed the overall function of the upper limbs irrespective of CRPS affected side, and the score ranges from 0 to 100. A higher QuickDASH score indicates greater disability of the upper limbs.

Body perception and motor dysfunction
The Bath CRPS Body Perception Disturbance Scale (Lewis & McCabe, 2010) and Foreign limb Feelings (FLF) questionnaire (Galer & Jensen, 1999) assessed self-perception of the CRPS affected limb. The Bath and FLF questionnaires scores range from 0 to 57 and 0 to 20, respectively. In addition, the FLF questionnaire assesses aspects of motor dysfunction such as involuntary movement. For both scales, a higher score indicates greater disturbance to self-perception of the CRPS affected limb.

2.4 | Tactile acuity (two-point discrimination)

Tactile acuity data of CRPS participants in this study have previously been published elsewhere (Di Pietro et al., 2020; Lee et al., 2020). Tactile acuity measures were not obtained from 3 of the 15 CRPS subjects due to extreme hand pain. The 2-point discrimination (TPD) test assessed tactile acuity and was performed immediately following the MRI. TPD is the ability to discriminate two distinct points touching the skin as two points and not one. The researcher applied a TPD wheel (Exacta™, CA) longitudinally to the distal pulp of the subject's index finger and asked the subject to report if they felt 1 point or 2 points touching their skin with each stimulation. The distances of 0 (i.e., 1 point), 2, 3, 4, and 5 mm between two points were applied seven times in a pseudo-randomized order, resulting in 35 trials per hand. The percentage of correct two-point perception versus distance between the points was fitted by a binary logistic regression (IBM SPSS Statistics for Windows, Version 24.0. Armonk, NY: IBM Corp.) to obtain individual psychometric functions of TPD for each subject's hand. The discrimination distance was determined at a 50% (chance) threshold of correct two-point perception. A higher discrimination distance indicates poorer tactile acuity.

2.5 | MRI data collection

All MRI data were collected in a 3 Tesla MRI scanner (Achieva TX, Philips Medical Systems) at Neuroscience Research Australia in Sydney, Australia. Each subject lay supine on the MRI scanner bed with their head immobilized in a padded 32-channel head coil. A high-resolution T1-weighted anatomical image of the whole brain in the sagittal plane was obtained (repetition time = 5600 ms; echo time = 2.5 ms, flip angle = 8°, raw voxel size 0.87 mm^3). Subjects were then asked to relax with their eyes closed as resting-state fMRI (rsfMRI) images were collected (series of 180 fMRI image volumes, gradient-echo echo-planar sequence with blood oxygen level-dependent contrast; repetition time = 2000 ms; echo time = 30 ms, flip angle = 90°, 37 axial slices, raw voxel size 3×3×4 mm).

2.6 | MRI data analysis

Image analysis was performed using SPM12 (Friston et al., 1995) and custom software. The T1 and rsfMRI images of the CRPS subjects with pain restricted to the left upper limb (or the more intense pain in the left upper limb) were left–right reflected across the midline on the y-axis before data processing. Hence, the brain's left hemisphere was contralateral to the CRPS affected limb in all 15 subjects. All fMRI images were then slice-time corrected, realigned and the Dynamic Retrospective Filtering (DRIFTER) toolbox (Särkkä et al., 2012) used to model and remove cardiac (frequency band of 60–120 beats per minute +1 harmonic) and respiratory (frequency band of 8–25 breaths per minute +1 harmonic) noise. LMRP detrending was used to remove movement-related signal changes. The linear model of the global signal (LMGS) method (Macey et al., 2004) was then used to remove global drifts in fMRI signal intensity. Each subject's fMRI images were then co-registered to the subject's own T1-weighted anatomical image. The T1 images were spatially normalized to Montreal Neurological Institute (MNI) space, and the normalization parameters were applied to the fMRI images sets to place them into MNI space. The resulting fMRI images were then smoothed using a 6 mm full-width at half-maximum (FWHM) Gaussian filter.

2.7 | Seeds

To explore regional specificity, we created multiple basal ganglia seeds (Figure 1a). First, we refined a left putamen seed (putamen ISO seed) from a previous study where we showed that ISO power was significantly greater in CRPS compared with control participants (Di Pietro et al., 2020). The putamen ISO seed for this current study

was refined to only include the putamen portion of a larger seed that originally encompassed the putamen and extended into the insular cortex. Second, we created four putamen seeds, each a 3 mm radius sphere and representative of: the motor hand (center X, Y, Z MNI coordinates: –28, –7, 2), motor foot (–28, –8, 6), motor tongue (–32, –8, –5), and SMA hand (–25, –7, 5) (Choi et al., 2012). Third, to elucidate the involvement of non-motor basal ganglia circuitry, we created six more seeds (3 mm radius spheres) representing the left caudate tail (visual processing loop; –29, –8, –17), caudate body (oculomotor loop; –15, –1, 18), ventrolateral (vl) caudate head (lateral orbitofrontal loop; –9, 10, 1), dorsolateral (dl) caudate head (dorsolateral prefrontal loop; –12, 10, 8), ventral putamen (default network loop; –29, –11, –10), and ventral striatum (limbic loop; –12, 11, –8) (Alexander et al., 1986; Choi et al., 2012; Middleton & Strick, 1996). In total, we created and assessed 11 basal ganglia seeds. In addition, to investigate basal ganglia functional connectivity, the fMRI analysis was restricted to cortical areas that receive input from the basal ganglia seeds (Alexander et al., 1986; Middleton & Strick, 1996) by applying a mask of the frontal lobe, anterior cingulate cortex (ACC), middle temporal gyrus, and parietal lobe (Figure 1b). All seeds were created in the left hemisphere; hence all seeds are contralateral to the CRPS affected limb.

2.8 | ISO analysis

We used the SPM Data Processing Assistant for Resting-State fMRI (DPARSF) toolbox (Chao-Gan & Yu-Feng, 2010) to calculate the amplitudes of low-frequency fluctuations (ALFFs), that is, power, of three standard ISO frequency ranges (slow-5: 0.01–0.027 Hz, slow-4: 0.027–0.073 Hz and slow-3: 0.073–0.198 Hz) defined by Buzsaki and Draguhn (2004) on the preprocessed fMRI image sets of control
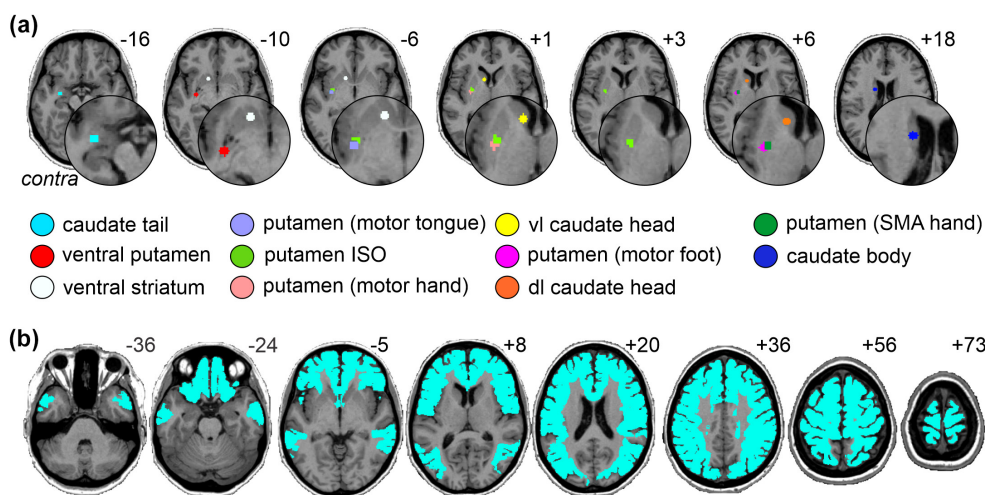
FIGURE 1 (a) Locations of the basal ganglia seeds used in the infraslow oscillation (ISO) and resting functional connectivity analysis. The seed regions are located contralateral to the CRPS affected limb. (b) The mask of the frontal lobe, anterior cingulate cortex, middle temporal gyrus, and parietal lobe used to restrict the functional connectivity analysis. Slice locations in Montreal neurological institute space are indicated on the top right of each axial slice. Contra, contralateral to affected limb; dl, dorsolateral; SMA, supplementary motor area; vl, ventrolateral

and CRPS subjects. The analysis was restricted to the 11 basal ganglia seeds to investigate ISO differences within the basal ganglia. Two-sample *t* tests were used to determine any differences between controls and CRPS subjects' slow-5, slow-4, and slow-3 ALFF power ($p < 0.05$, two-tailed). The slow-5, slow-4, and slow-3 mean±SEM ALFF power for controls and CRPS subjects were plotted for each seed. For seeds that were significantly different between controls and CRPS subjects, Pearson's correlations ($p < 0.05$, two-tailed) were performed between CRPS subjects' ALFF power and pain duration, pain intensity, questionnaire scores, and tactile acuity, using GraphPad Prism 9.1 (GraphPad Software, Inc., San Diego, CA). The D'Agostino-Pearson normality test confirmed the normal distribution of pain, questionnaire, and tactile acuity data before correlation analysis. To account for multiple comparisons for each seed and each ISO frequency range, the Benjamini and Hochberg method (Benjamini & Hochberg, 1995) was used to calculate false discovery rate (FDR)-adjusted *p* values at 5% FDR.

2.9 | Seed-based connectivity analysis

For each of the 11 basal ganglia seeds, the mean signal intensity at each time point was calculated and averaged over the entire seed. Relationships between signal intensity changes and the signal intensity changes in each voxel of the brain were then determined for each seed in each subject. The resultant resting-state connectivity strength brain maps were then smoothed using a 6 mm FWHM Gaussian filter and second-level random-effects analysis was performed to determine significant differences between CRPS and control groups ($p < 0.05$, FDR corrected for multiple comparisons, minimum contiguous cluster size of 20 voxels). For the resting-state connectivity analysis of the putamen ISO seed, the beta value (connectivity strength effect size) of each significant cluster was extracted, and the mean±SEM plotted. In addition, for the CRPS subjects, linear relationships between these beta values and pain duration, pain intensity, questionnaire scores, and tactile acuity data were determined using Pearson's correlations ($p < 0.05$, two-tailed) and the Benjamini and Hochberg method (Benjamini & Hochberg, 1995) was used to calculate FDR-adjusted *p* values at 5% FDR. One-sample one-sided *t* tests were performed within groups for each basal ganglia seed (see Supporting Information).

3 | RESULTS

3.1 | CRPS subject characteristics

Individual CRPS subject characteristics are reported in Table 1. The CRPS subjects' average pain duration was 4.6±0.9 years (mean±SEM). All 15 CRPS subjects reported ongoing pain in the upper limb, with 12 of the 15 subjects reporting upper limb pain restricted to one side (10 right, 2 left). Three subjects reported bilateral upper limb pain (2 reporting greater pain in the right upper limb

and 1 on the left). Seven CRPS subjects also reported pain in the lower limb. CRPS subjects' motor signs, questionnaire scores, and tactile acuity data are reported in Table 2. Thirteen CRPS subjects displayed motor signs on the day of the study;10 CRPS subjects presented with weakness, 2 with dystonia, 1 with tremor, and 1 with rigidity. CRPS subjects reported an average pain intensity of 5.3±0.5 for day pain and 4.6±0.6 for diary pain.

3.2 | ISOs

As expected, for the putamen ISO seed, the CRPS group displayed significantly greater slow-4 ALFF (0.027–0.073 Hz) power than controls (mean±SEM, CRPS: 1.06±0.06, controls: 0.85±0.03, $p < 0.001$) (Figure 2a). The putamen ISO seed also displayed significantly greater slow-3 ALFF (0.073–0.198 Hz) power in the CRPS group (CRPS: 1.11±0.09, controls: 0.88±0.03, $p = 0.003$). This result was regionally specific; only 3 of the remaining 10 basal ganglia seeds displayed significant differences in ALFF power between groups. Namely, the putamen SMA hand, motor hand, and motor tongue area seeds demonstrated greater CRPS slow-4 ALFF power in CRPS than controls (SMA hand: CRPS: 0.93±0.06, controls: 0.81±0.03, $p = 0.046$; motor hand: CRPS: 1.06±0.08, controls: 0.86±0.03, $p = 0.005$; motor tongue: CRPS: 1.03±0.07, controls: 0.84±0.03, $p = 0.004$) (Figure 2b). There were no significant differences in slow-4 ALFF power for the remaining seven seeds or for either slow-3 or slow-5 (0.01–0.027 Hz) frequency bands in any basal ganglia seed, apart from the putamen ISO seed.

In CRPS subjects, increased ISO power of the putamen was correlated with pain and functional disability (Table 3). A lower PRWHE function score, indicating better wrist function of the CRPS affected hand, correlated with increased slow-4 ALFF power of the putamen ISO seed (Figure 3a) and putamen motor hand (Figure 3b). A lower QuickDASH score, indicating less functional disability of the upper limbs, correlated with increased slow-4 putamen motor hand (Figure 3c), putamen motor tongue, and slow-3 putamen motor hand (Figure 3d) ALFF power.

3.3 | Functional connectivity

For each of the 11 basal ganglia seeds, significant differences in resting-state functional connectivity strengths between CRPS and control groups were determined. In no region was connectivity strength greater in controls than in CRPS subjects. For the putamen ISO seed, CRPS subjects displayed significantly greater connectivity strengths compared with controls in the ipsilateral and contralateral primary motor cortices (M1) in the region innervating the lower limbs (mean±SEM beta values: ipsilateral M1: CRPS 0.13±0.02, controls 0.02±0.02; contralateral M1: CRPS 0.15±0.02, controls 0.03±0.01), contralateral M1 in the upper limb and hand region (CRPS: 0.13±0.02, controls 0.02±0.01), contralateral cingulate motor area (CMA; CRPS 0.16±0.02, controls 0.05±0.02),

TABLE 1 CRPS subject demographics, medical history, and medication

Subject	Age	Sex	Pain duration (years)	CRPS affected region(s)	Inciting event	Medications	Comorbidities Pain-related	Non-pain-related
1	49.2	M	7.0	R UL, R LL, L LL, face, abdomen	Pain in R hand	Turmeric tablets	None	None
2	56.4	F	4.2	L UL, R UL, R LL, R and L chest	L humerus fracture	Duloxetine, gabapentin, oxycodone, quetiapine, tapentadol	L radial nerve palsy, triangular fibrocartilage complex degeneration of R hand	None
3	55.8	F	0.9	R UL, R neck, R chest	Spontaneous onset	Ashwagandha, budesonide, cannabis, codeine, formoterol, oxycodone, paracetamol, salbutamol	Back pain, fibromyalgia, osteoarthritis, radiculopathy, spinal disc herniation	COPD, peptic ulcer, Raynaud's disease
4	61.7	F	6.2	L UL, R UL	R hand tendon release surgery	Amitriptyline, cannabidiol drops, codeine, levothyroxine, magnesium, paracetamol, topiramate, tramadol, valerian	None	Diverticulitis, gastro-esophageal reflux disease, Graves' disease (thyroidectomized)
5	58.1	F	8.7	R UL, R LL, R face	R arm surgery	Codeine, duloxetine, linagliptin, meloxicam, metformin, paracetamol	None	Diabetes
6	66.6	F	9.5	R UL, L UL, R LL, L LL	R radius fracture	Amlodipine, gabapentin, ketamine in lipoderm cream, metformin, metoprolol, pantoprazole, salbutamol	Osteoarthritis	Asthma, diabetes, gastric reflux, hypertension, pubic symphysitis, supraventricular tachycardia
7	46.8	M	1.5	R UL	Spontaneous onset	Amlodipine, atorvastatin, ibuprofen, paracetamol, perindopril, pregabalin	None	Hyperlipidemia, hypertension
8	34.2	F	5.3	R UL, R LL, R hip	R wrist fracture	Amitriptyline, buprenorphine patch	Migraine, R hip bursitis	None
9	25.9	F	1.3	R UL, L and R neck, spine, L LL	R hand nerve damage	None	Endometriosis	Polycystic ovarian syndrome
10	45.2	M	1.2	R UL	R wrist injury	Codeine, ibuprofen, magnesium, pregabalin, topical rub (containing copaiba, frankincense, peppermint, coconut oil), vitamin B, vitamin C	Bell's palsy, bulging discs	None
11	45.9	F	3.9	L UL	L hand carpal tunnel release surgery	Amitriptyline, betahistine, duloxetine, naproxen, pantoprazole, rizatriptan, tapentadol, valaciclovir	Carpal tunnel of R hand, fibromyalgia, migraine	Herpes, polycystic ovarian syndrome with insulin resistance, vertigo
12	23.8	F	2.6	R UL, L UL	Overload	Amitriptyline, gabapentin, levothyroxine	None	Hashimoto's disease

TABLE 1 (Continued)

Subject	Age	Sex	Pain duration (years)	CRPS affected region(s)	Inciting event	Medications	Comorbidities Pain-related	Non-pain-related
13	52.3	F	2.9	**R UL**, R torso	Broke tailbone	Ashwagandha, fish oil, ibuprofen, magnesium, mega B, melatonin, paracetamol, tapentadol, vitamin C, vitamin D	Endometriosis	None
14	37.8	F	12.7	**R UL**, R neck, L LL	Spontaneous onset	Duloxetine, gabapentin, naloxone, oxycodone, palmitoylethanolamide (PEA)	Endometriosis, endosalpingiosis	Raynaud's disease
15	52.3	M	1.9	**R UL**, L and R neck, back	R scaphoid fusion surgery	Cholecalciferol, ibuprofen, magnesium, oxycodone, paracetamol, pregabalin, tramadol, venlafaxine, zopiclone	L shoulder bursitis	Sleep apnea
Mean (±SEM)	47.5 (±3.2)		4.6 (±0.9)					

Note: The CRPS region with the most severe pain is in bold. CRPS regions that are in remission are in *italics*. Medication taken in the last 24 h of the day of testing are underlined.

Abbreviations: L, left; LL, lower limb; R, right; SEM, standard error of mean; UL, upper limb.

ipsilateral primary somatosensory cortex (S1) in the hand region (CRPS 0.11 ± 0.02, controls 0.004 ± 0.01), ipsilateral supramarginal gyrus (CRPS 0.17 ± 0.02, controls 0.04 ± 0.01), ipsilateral pars opercularis (CRPS 0.19 ± 0.02, controls 0.04 ± 0.02), ipsilateral orbitofrontal cortex (CRPS 0.14 ± 0.02, controls 0.02 ± 0.01), and in the contralateral middle temporal gyrus (CRPS 0.13 ± 0.03, controls 0.01 ± 0.01) (Figure 4 and Table 4). In CRPS subjects, the connectivity between the putamen ISO seed and the ipsilateral OFC was positively correlated with day pain ($r = 0.60$) and putamen ISO and contralateral M1 hand area was positively correlated with a higher foreign limb feelings (FLF) questionnaire score ($r = 0.62$), however, neither correlations were significant after multiple comparisons adjustment.

Analysis of the remaining 10 basal ganglia seeds revealed that 5 seeds displayed significant connectivity increases in the CRPS group, 4 of which were putamen motor loop seeds. Similar to the putamen ISO seed, the putamen motor hand seed in CRPS subjects displayed greater resting connectivity strengths than controls with: the ipsilateral M1 lower limb region (mean $\pm$ SEM beta values: CRPS 0.14 ± 0.02, controls 0.04 ± 0.01), ipsilateral and contralateral M1 hand region (ipsilateral: CRPS 0.16 ± 0.02, controls 0.05 ± 0.01; contralateral: CRPS 0.16 ± 0.03, controls 0.04 ± 0.01), contralateral CMA (CRPS 0.17 ± 0.03, controls 0.05 ± 0.01), ipsilateral OFC (CRPS 0.13 ± 0.03, controls 0.02 ± 0.01), and the ipsilateral angular gyrus (CRPS 0.16 ± 0.02, controls 0.04 ± 0.01) (Figure 5a, Table 4). Similarly, for the putamen motor foot seed analysis, CRPS subjects also displayed significantly greater connectivity strengths in the ipsilateral M1 hand region (CRPS 0.17 ± 0.03, controls 0.04 ± 0.01), contralateral M1 hand region (CRPS 0.17 ± 0.04, controls 0.04 ± 0.02), ipsilateral M1 face region (CRPS 0.08 ± 0.01, controls 0.01 ± 0.01), ipsilateral and contralateral CMA (ipsilateral: CRPS 0.13 ± 0.03, controls 0.01 ± 0.01; contralateral: CRPS 0.20 ± 0.03, controls 0.06 ± 0.01), ipsilateral angular gyrus (CRPS 0.18 ± 0.04, controls 0.01 ± 0.02), and in the ipsilateral supramarginal gyrus (CRPS 0.18 ± 0.03, controls 0.04 ± 0.02) (Figure 5b, Table 4). In contrast, connectivity strength for the putamen motor tongue seed was only greater in CRPS subjects compared with controls in a discrete region of the ipsilateral frontal cortex (CRPS 0.18 ± 0.02, controls 0.01 ± 0.02) (Figure 5c, Table 4). For the putamen SMA hand seed, CRPS subjects displayed greater connectivity than controls in the contralateral CMA (CRPS 0.14 ± 0.02, controls 0.03 ± 0.01), ipsilateral OFC (CRPS 0.11 ± 0.03, controls 0.004 ± 0.01), contralateral M1 hand area (CRPS 0.15 ± 0.03, controls 0.05 ± 0.01), ipsilateral M1 tongue area (CRPS 0.13 ± 0.03, controls 0.01 ± 0.01), ipsilateral angular gyrus (CRPS 0.16 ± 0.03, controls 0.05 ± 0.01), ipsilateral and contralateral supramarginal gyrus (ipsilateral: CRPS 0.16 ± 0.02, controls 0.03 ± 0.01; contralateral: CRPS 0.13 ± 0.03, controls 0.01 ± 0.02), contralateral frontal cortex (CRPS 0.11 ± 0.03, controls 0.01 ± 0.02), and the contralateral middle temporal gyrus (CRPS 0.11 ± 0.02, controls 0.03 ± 0.01) (Figure 5d, Table 4).

The caudate body seed was the only non-motor region in which resting functional connectivity was significantly different between

TABLE 2 CRPS subjects' motor signs, questionnaire scores, and tactile acuity

Subject	Motor signs	Pain intensity		PRWHE				Bath	FLF	TPD (mm)	
		Day pain	Diary pain	Pain score	Function score	Total score	QuickDASH			Affected hand	Unaffected hand
1	Tremor, dystonia	4.0	4.5	32	30.5	62.5	81.8	34	18	3.8	1.6
2	Rigidity	7.8	8.1	45	30.5	75.5	75.0	29	16	–	–
3	Weakness	7.9	8.3	46	38	84	75.0	39	12	3.7	3.3
4	Weakness	4.3	5.8	42	46	88	54.5	3	6	2.7	1.6
5	Weakness	4.1	4.7	43	40.5	83.5	75.0	32	19	4.1	2.3
6	Weakness	5.0	3.7	26	26.5	52.5	56.8	10	5	4.1	3.3
7	Weakness	7.1	6.8	41	37	78	75.0	12	4	2.1	1.8
8	Weakness	2.4	4.3	28	33.2	61.2	31.8	19	15	3.7	2.4
9	Weakness	6.8	5.4	40	36.5	76.5	75.0	18	2	2.6	2.2
10	Weakness	3.0	2.0	38	38	76	79.5	18	11	–	–
11	–	5.6	0.6	5	8.5	13.5	25.0	29	3	2.3	1.9
12	Weakness	4.4	4.5	28	16.5	44.5	47.7	21	0	2.5	2.7
13	–	3.5	3.8	28	15.5	43.5	54.5	30	11	4.1	2.7
14	Weakness	5.9	0.0	23	21	44	54.5	25	7	2.0	1.9
15	Dystonia	7.6	7.0	46	47	93	88.6	26	16	–	–
Mean (±SEM)		5.3 (±0.5)	4.6 (±0.6)	34.1 (±2.9)	31.0 (±2.9)	65.1 (±5.6)	63.3 (±4.8)	23.0 (±2.5)	9.7 (±1.6)	3.1 (±0.2)	2.3 (±0.2)

Abbreviations: Bath, bath CRPS body perception disturbance scale; FLF, foreign limb feelings; PRWHE, patient-rated wrist and hand evaluation; QuickDASH, shortened disabilities of the arm, shoulder and hand; SEM, standard error of mean; TPD, two-point discrimination.
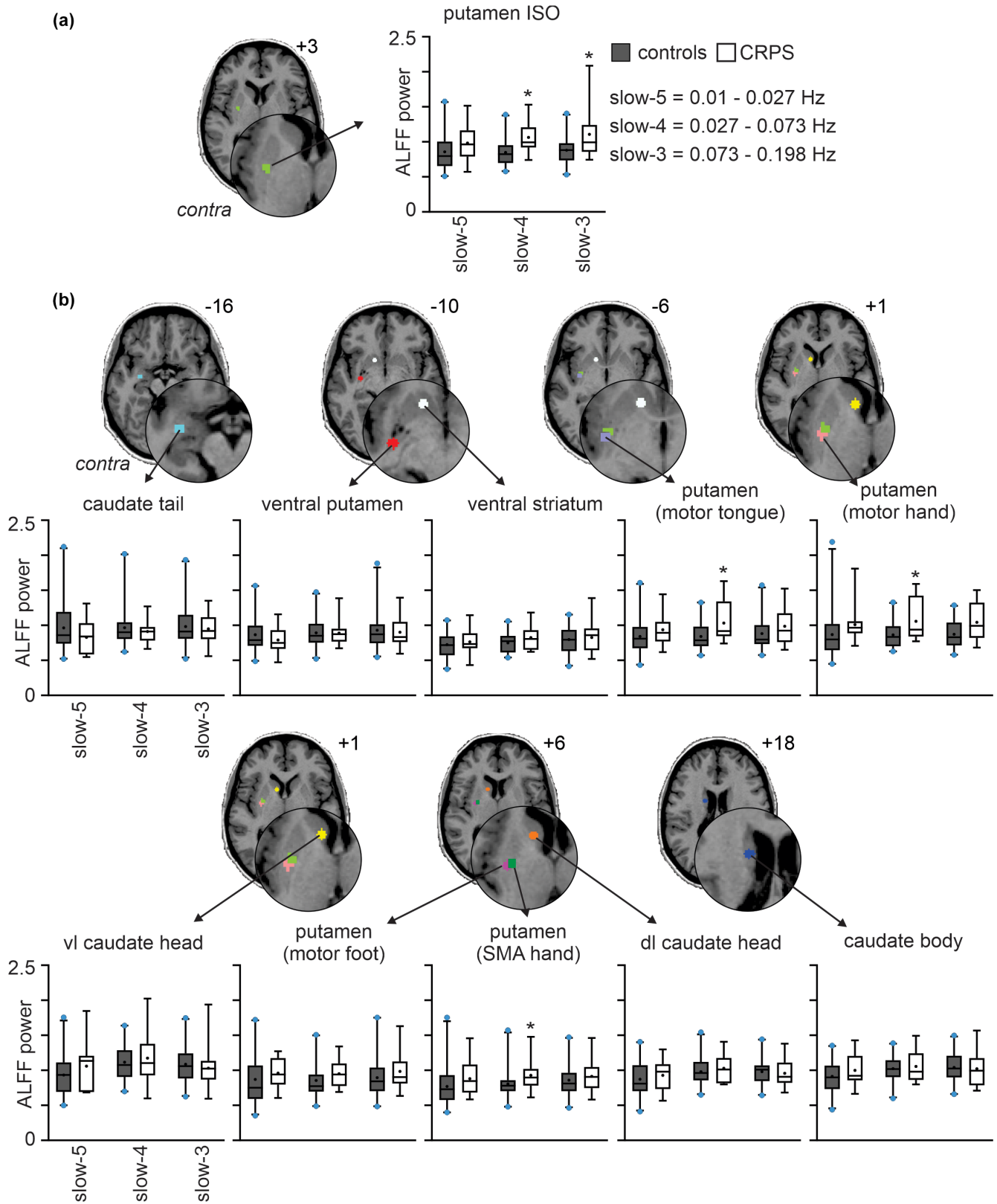
CRPS subjects and controls (Figure 6, Table 4). CRPS subjects displayed greater connectivity strength than controls in several brain regions, including the ipsilateral OFC (CRPS 0.13±0.03, controls 0.02±0.01), ipsilateral and contralateral dorsolateral prefrontal cortex (dlPFC; ipsilateral: CRPS 0.15±0.01, controls 0.04±0.01; contralateral: CRPS 0.17±0.02, controls 0.06±0.02), ipsilateral and contralateral mid-cingulate cortex (MCC; ipsilateral: CRPS 0.17±0.01, controls 0.07±0.01; contralateral: CRPS 0.15±0.02, controls 0.02±0.01), ipsilateral and contralateral superior parietal cortex (ipsilateral: CRPS 0.16±0.04, controls 0.03±0.02;

FIGURE 2 Increased infraslow oscillations (ISO) in CRPS subjects as compared with matched healthy controls. Box and whisker plots of mean amplitude of low-frequency fluctuations (ALFF) power over three standard ISO frequency bands: Slow-5: 0.01–0.027 Hz, slow-4: 0.027–0.073 Hz and slow-3: 0.073–0.198 Hz in the region of the (a) putamen ISO and (b) caudate tail, ventral putamen, ventral striatum, motor tongue area of the putamen, motor hand area of the putamen, ventrolateral (vl) caudate head, motor foot area of the putamen, supplementary motor hand area of the putamen (SMA hand), dorsolateral (dl) caudate head and caudate body seeds. The seed regions are located contralateral to the CRPS affected limb. The box indicates the interquartile range: The median is indicated by the solid line inside the box, the 25th percentile by the bottom line of the box and 75th percentile by the top line of the box. The mean is represented by the black dot within the box. The whiskers extend from the 2.5th to 97.5th percentile. The blue dots above and below the whiskers represent data points that lie outside the 2.5–97.5 percentile range. Slice locations in Montreal Neurological Institute space are indicated on the top right of each axial slice. Contra: Contralateral to affected limb. (*$p < 0.05$ significantly different to controls; two-sample t test)

TABLE 3 Correlations between infraslow oscillation power and questionnaire scores

| Seed	Correlated questionnaire scores	Pearson r	p value
Slow 4			
Putamen ISO	PRWHE pain score	−0.7289	0.0137
	PRWHE function score	−0.6728	0.0260
	PRWHE total score	−0.7275	0.0137
Putamen motor hand	PRWHE pain score	−0.7593	0.0130
	PRWHE function score	−0.6406	0.0328
	PRWHE total score	−0.7264	0.0143
	QuickDASH	−0.7023	0.0152
Putamen motor tongue	PRWHE pain score	−0.7436	0.0098
	PRWHE total score	−0.6604	0.0321
	QuickDASH	−0.7901	0.0065
Slow 3			
Putamen motor hand	PRWHE pain score	−0.6951	0.0442
	PRWHE total score	−0.5993	0.0789
	QuickDASH	−0.6656	0.0442

Note: All seeds are contralateral to the CRPS affected limb. The Pearson's correlation coefficient (r) and the FDR-adjusted significance of correlation (p) are reported.

Abbreviations: PRWHE, patient-rated wrist and hand evaluation; QuickDASH, shortened disabilities of the arm, shoulder and hand.

contralateral: CRPS 0.19 ± 0.02, controls 0.08 ± 0.02), contralateral superior frontal cortex (CRPS 0.15 ± 0.02, controls 0.04 ± 0.01), contralateral anterior cingulate cortex (ACC; CRPS 0.17 ± 0.02, controls 0.06 ± 0.01), contralateral supramarginal gyrus (CRPS 0.17 ± 0.04, controls 0.05 ± 0.02), ipsilateral and contralateral M1 (ipsilateral: CRPS 0.13 ± 0.03, controls 0.02 ± 0.02; contralateral: CRPS 0.13 ± 0.03, controls 0.01 ± 0.02), ipsilateral and contralateral angular gyrus (ipsilateral: CRPS 0.17 ± 0.03, controls 0.05 ± 0.02; contralateral: CRPS 0.16 ± 0.04, controls 0.03 ± 0.02), ipsilateral and contralateral piriform cortex (ipsilateral: CRPS 0.14 ± 0.02, controls 0.04 ± 0.01; contralateral: CRPS 0.12 ± 0.02, controls 0.02 ± 0.01), ipsilateral and contralateral middle temporal gyrus (ipsilateral: CRPS 0.13 ± 0.02, controls 0.04 ± 0.01; contralateral: CRPS 0.12 ± 0.02, controls 0.03 ± 0.01). No significant functional connectivity strength differences were found for the non-motor regions, caudate tail, dl caudate head, vl caudate head, ventral striatum, and ventral putamen seeds.

4 | DISCUSSION

Consistent with our hypothesis, we report significant differences in both basal ganglia ISO power and basal ganglia functional connectivity between individuals with CRPS and pain-free controls. These differences are primarily restricted to the motor basal ganglia loops, particularly regions that represent the upper limb, with one exception being the caudate body oculomotor loop. More specifically, we found increased ISO power in CRPS subjects in putamen divisions representative of the SMA hand, motor hand, and motor tongue. In addition to the putamen SMA hand, motor hand, motor tongue seeds, the putamen motor foot, and caudate body seeds displayed significantly greater (than controls) resting connectivity strength to multiple basal ganglia-cortical input areas such as M1, SMA, CMA, and OFC in CRPS subjects. These results highlight alterations in basal ganglia function at rest in CRPS and likely underpin the alterations in motor control commonly seen in this condition.
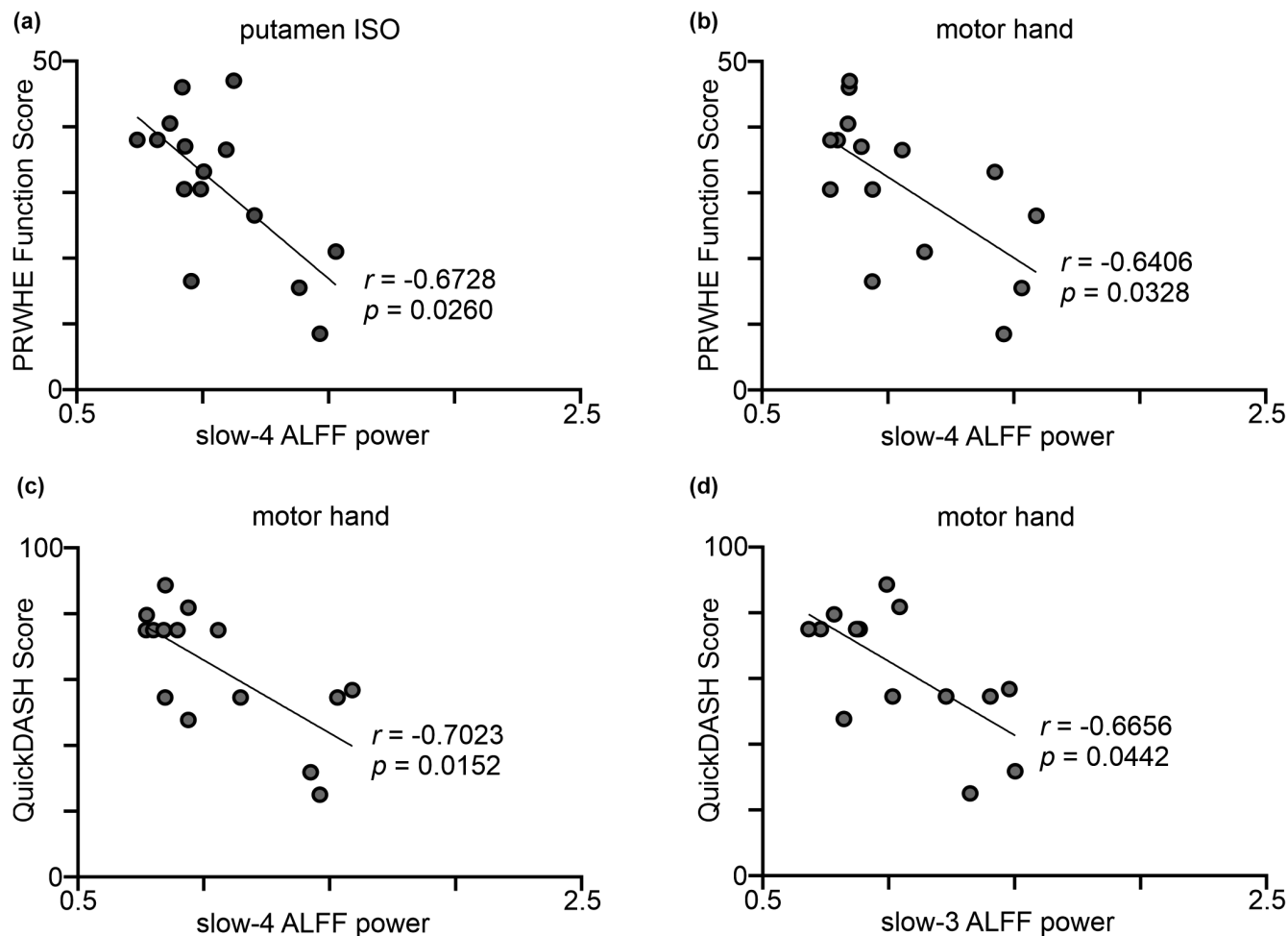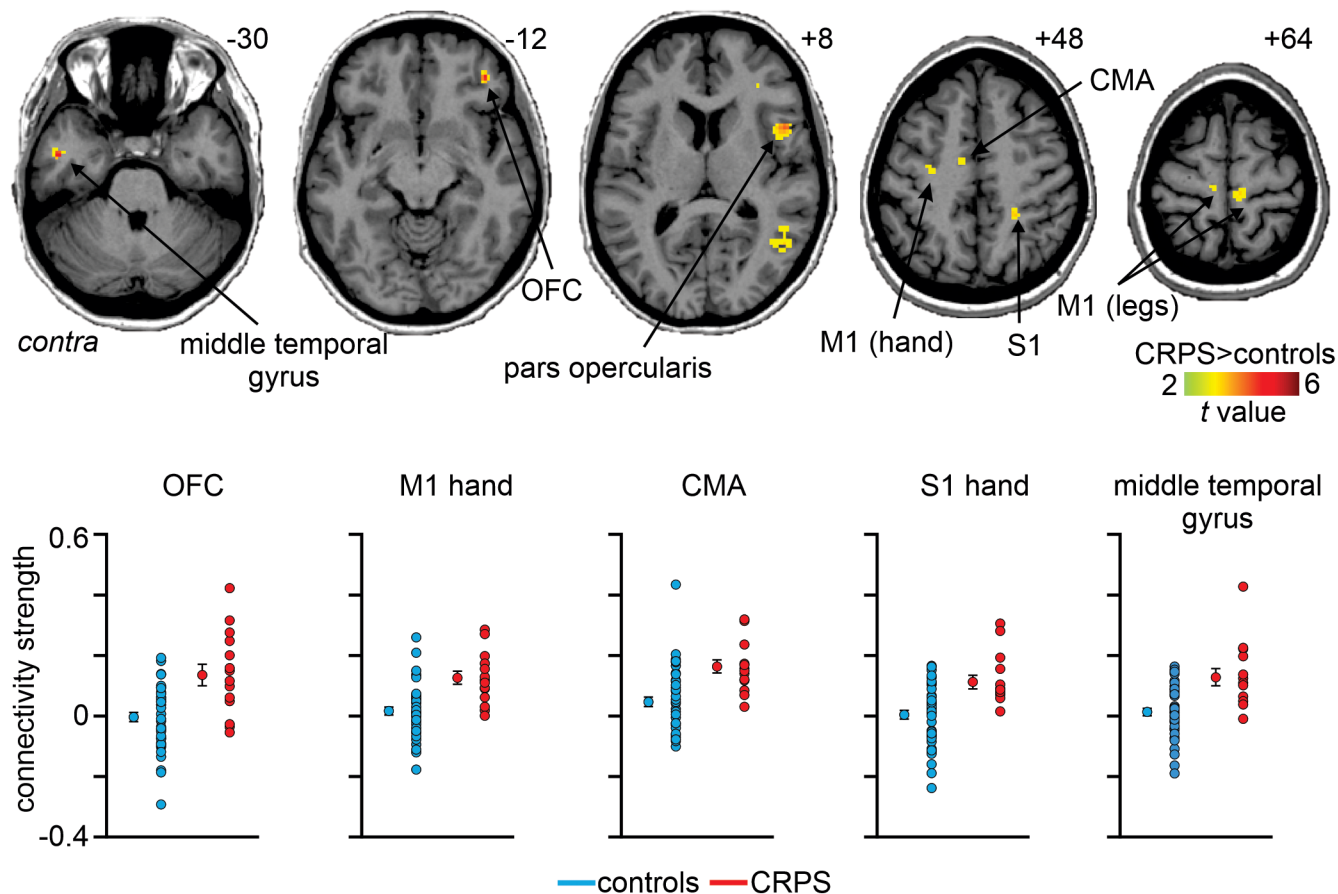
FIGURE 3 Increased infraslow oscillations (ISO) power in CRPS subjects correlated with less disability. Scatter plots showing Pearson correlations; the line represents the best fit for the correlations. The Pearson's correlation coefficient (*r*) and the FDR-adjusted significance of correlation (*p*) are displayed on the plots. Patient-rated wrist and hand evaluation (PRWHE) correlated with slow-4 ALFF power of the (a) putamen ISO seed and (b) putamen motor hand area. Shortened disabilities of the arm, shoulder and hand (QuickDASH) outcome measure correlated with (c) slow-4 ALFF power, and (d) slow-3 ALFF power of the putamen motor hand area

We found greater putaminal ISO power, primarily of the slow-4 bandwidth, which includes the 0.03–0.06 Hz range, a range we have previously reported on (Di Pietro et al., 2020). This range coincides with the astrocytic calcium wave propagation frequency range and subsequent astrocytic gliotransmitter release (Cornell-Bell et al., 1990; Crunelli et al., 2002) and we have hypothesized that increased ISOs found in CRPS and other forms of chronic neuropathic pain may be due to chronic astrogliosis (Henderson & Di Pietro, 2016). While no investigation has explored chronic astrogliosis in the putamen of CRPS patients, a postmortem study reported chronic astrogliosis in the spinal cord dorsal horn in CRPS (Del Valle et al., 2009). Furthermore, two human positron emission tomography studies have reported increased putaminal translocator protein binding in CRPS, a marker that binds to microglia and potentially also astrocytes (Jeon et al., 2017; Seo et al., 2021). Given this, we now propose that astrogliosis may also contribute to motor dysfunction in CRPS. Indeed, in mice, artificial elevation of calcium through activation of GFAP+ glial cells (astrocytes) in the brain and spinal cord

resulted in motor coordination impairment (Agulhon et al., 2013). From the results of this current study, we speculate that astrogliosis within the basal ganglia is specific to the areas of greater slow-4 oscillations found in CRPS subjects, namely putamen SMA hand, motor hand, and motor tongue areas contralateral to the CRPS affected limb. Supporting this idea is evidence of elevated pro-inflammatory cytokine levels in the striatum of rats with chronic neuropathic pain (Al-Amin et al., 2011; Apkarian et al., 2006; Fiore & Austin, 2016). We also identified greater CRPS slow-3 oscillations in the putamen and motor hand area of the putamen contralateral to the CRPS affected limb. This suggests that in addition to calcium wave elevation and astrogliosis, there are other aberrant mechanisms that contribute to the motor dysfunction seen in CRPS.

In addition to altered resting oscillation patterns, we report significant increases in resting putamen connectivity. The putamen is the input region of the basal ganglia motor loop; it is organized somatotopically and has segregated inputs from M1 and SMA (Alexander et al., 1986; Nambu et al., 2002). Activity fluctuations in

FIGURE 4 Significantly greater functional connectivity strength of the putamen infraslow oscillations (ISO) seed in CRPS subjects as compared to controls ($p < 0.05$; false discovery rate corrected for multiple comparisons, hot color scale). Slice locations in Montreal neurological institute space are indicated on the top right of each axial slice. Lower panel are plots of individual subject and mean ± SEM beta values of putamen ISO seed connectivity to the orbitofrontal cortex (OFC), hand area of the primary motor cortex (M1 hand), cingulate motor area (CMA), hand area of the somatosensory cortex (S1 hand), and middle temporal gyrus. Contra, contralateral to affected limb

the putamen motor hand, motor foot and SMA hand areas displayed greater synchrony with cortical areas in CRPS subjects. Overall, these areas showed stronger coupling with other motor related cortical regions such as the M1 region innervating the body as well as the CMA. Our findings of altered bilateral putamen-M1 connectivity are consistent with the bilateral nature of M1 changes in CRPS (Di Pietro et al., 2013a; Maihöfner et al., 2007). Contralateral changes are hypothesized to be due to altered functioning of the affected limb and ipsilateral changes related to compensatory use of the unaffected limb (Azqueta-Gavaldon et al., 2020). Consistent with this, we found that increased contralateral putamen-M1 hand functional connectivity was correlated with higher FLF scores in CRPS, indicating a greater self-perceived disturbance in motor function and neglect-like feelings of the CRPS affected limb. In Parkinson's disease and CRPS, greater putamen-M1 connectivity predicts poorer motor performance in a pegboard task that requires fast and accurate motor coordination (Azqueta-Gavaldon et al., 2020; Simioni et al., 2015). Furthermore, in CRPS, decreased putamen-M1 functional connectivity correlated with reduced forearm range of motion (Azqueta-Gavaldon et al., 2020). Thus, the increased putamen-M1

hand functional connectivity in CRPS subjects may underlie motor dysfunction.

As well as altered connectivity to well-described motor cortical regions, we found increased putamen connectivity with frontal and parietal association cortices, consistent with putamen anatomical connectivity to those areas (Jarbo & Verstynen, 2015). We found increased connectivity of the putamen ISO and putamen SMA hand seeds with the OFC, an important brain area in emotion and reward. Increased OFC connectivity is associated with non-reward, punishment, and depression (Rolls et al., 2020) and the increased putamen-OFC connectivity found in the current study may underpin the aversion to movement commonly seen in CRPS. Our study demonstrated increased putamen motor hand, motor foot, and SMA hand connectivity to the parietal cortex, mainly the inferior parietal lobule (IPL; formed by the supramarginal and angular gyri). The IPL's role involves sensorimotor integration, motor planning, spatial and nonspatial attention, and motor preparation (Caspers et al., 2013). In CRPS, finger tapping on the CRPS affected side increased IPL activation compared to the unaffected cerebral hemisphere and also to healthy controls (Schwenkreis et al., 2009), and in CRPS

TABLE 4 Montreal neurological institute (MNI) coordinates, *t*-scores, cluster size, and beta values for regions with significant functional connectivity differences between CRPS subjects and healthy controls

Region	Side	MNI coordinates			t-score	Cluster size	Beta values (mean ± SEM)	
		X	Y	Z			CRPS	Controls
Putamen ISO seed CRPS > Controls								
Primary motor cortex (M1) leg area	ipsi	8	−28	64	3.75	21	0.13 ± 0.02	0.02 ± 0.02
Primary motor cortex (M1) leg area	contra	−10	−24	58	4.33	53	0.15 ± 0.02	0.03 ± 0.01
Primary motor cortex (M1) hand area	contra	−30	−18	54	4.37	59	0.13 ± 0.02	0.02 ± 0.01
Cingulate motor area (CMA)	contra	−4	−8	54	3.95	31	0.16 ± 0.02	0.05 ± 0.02
Primary somatosensory (S1) hand area	ipsi	24	−42	48	3.83	23	0.11 ± 0.02	0.004 ± 0.01
Supramarginal gyrus	ipsi	46	−42	38	4.86	555	0.17 ± 0.02	0.04 ± 0.01
Pars opercularis	ipsi	48	10	8	4.30	156	0.19 ± 0.02	0.04 ± 0.02
Orbitofrontal cortex (OFC)	ipsi	30	34	0	4.66	26	0.14 ± 0.04	−0.003 ± 0.02
Orbitofrontal cortex (OFC)	ipsi	40	42	−12	4.60	38	0.14 ± 0.02	0.02 ± 0.01
Middle temporal gyrus	contra	−46	−6	−30	4.84	23	0.13 ± 0.03	0.01 ± 0.01
Putamen (motor hand) seed CRPS > Controls								
Primary motor cortex (M1) leg area	ipsi	6	−30	62	4.25	26	0.14 ± 0.02	0.04 ± 0.01
Primary motor cortex (M1) hand area	ipsi	36	−8	50	4.75	35	0.16 ± 0.02	0.05 ± 0.01
Primary motor cortex (M1) hand area	contra	−32	−10	48	4.50	93	0.16 ± 0.03	0.04 ± 0.01
Cingulate motor area (CMA)	contra	−8	−8	50	4.34	59	0.17 ± 0.03	0.05 ± 0.01
Angular gyrus	ipsi	34	−70	22	4.75	82	0.16 ± 0.02	0.04 ± 0.01
Angular gyrus	ipsi	42	−62	8	4.01	81	0.18 ± 0.03	0.05 ± 0.02
Orbitofrontal cortex (OFC)	ipsi	38	42	−14	4.32	32	0.13 ± 0.03	0.02 ± 0.01
Putamen (motor foot) seed CRPS > Controls								
Primary motor cortex (M1) hand area	ipsi	22	−16	62	3.74	41	0.16 ± 0.03	0.02 ± 0.02
Primary motor cortex (M1) hand area	ipsi	38	−8	50	4.58	82	0.17 ± 0.03	0.04 ± 0.01
Primary motor cortex (M1) hand area	contra	−32	−10	46	3.57	26	0.17 ± 0.04	0.04 ± 0.02
Primary motor cortex (M1) face area	ipsi	62	10	18	3.50	21	0.08 ± 0.01	0.01 ± 0.01
Cingulate motor area (CMA)	ipsi	20	−4	54	3.81	26	0.13 ± 0.03	0.01 ± 0.01
Cingulate motor area (CMA)	contra	−10	−8	50	4.60	89	0.20 ± 0.03	0.06 ± 0.01
Supramarginal gyrus	ipsi	54	−36	30	4.01	64	0.18 ± 0.03	0.04 ± 0.02
Angular gyrus	ipsi	34	−70	22	4.21	54	0.19 ± 0.03	0.05 ± 0.02
Angular gyrus	ipsi	54	−66	18	4.10	24	0.12 ± 0.03	−0.003 ± 0.02
Angular gyrus	ipsi	46	−50	10	4.23	81	0.18 ± 0.04	0.01 ± 0.02
Putamen (motor tongue) seed CRPS > Controls								
Frontal cortex	ipsi	26	8	48	5.76	25	0.18 ± 0.02	0.01 ± 0.02
Putamen (SMA hand) seed CRPS > Controls								
Cingulate motor area (CMA)	contra	−10	−10	48	4.31	33	0.14 ± 0.02	0.03 ± 0.01
Superior frontal cortex	contra	−6	48	38	3.76	24	0.11 ± 0.03	0.01 ± 0.02
Primary motor cortex (M1) hand area	contra	−30	−10	46	4.13	33	0.15 ± 0.03	0.05 ± 0.01

(Continues)

TABLE 4 (Continued)

Region	Side	MNI coordinates			t-score	Cluster size	Beta values (mean ± SEM)	
		X	Y	Z			CRPS	Controls
Primary motor cortex (M1) tongue area	ipsi	50	−6	30	3.94	42	0.13 ± 0.03	0.01 ± 0.01
Supramarginal gyrus	contra	−40	−60	26	3.60	20	0.13 ± 0.03	0.01 ± 0.02
Supramarginal gyrus	ipsi	52	−36	22	4.98	294	0.16 ± 0.02	0.03 ± 0.01
Angular gyrus	ipsi	36	−70	24	4.08	35	0.16 ± 0.03	0.05 ± 0.01
Orbitofrontal cortex (OFC)	ipsi	32	18	−18	4.04	39	0.11 ± 0.03	0.004 ± 0.01
Middle temporal gyrus	contra	−52	−2	−32	4.21	38	0.11 ± 0.02	0.03 ± 0.01
Caudate body seed CRPS > Controls								
Superior parietal cortex	ipsi	22	−54	68	3.18	51	0.10 ± 0.03	0.01 ± 0.01
Superior parietal cortex	ipsi	4	−52	62	3.36	31	0.16 ± 0.03	0.04 ± 0.02
Superior parietal cortex	ipsi	18	−56	58	2.97	25	0.11 ± 0.03	0.01 ± 0.02
Superior parietal cortex	contra	−28	−56	40	3.07	80	0.19 ± 0.02	0.08 ± 0.02
Superior parietal cortex	contra	−14	−78	34	3.15	27	0.17 ± 0.03	0.06 ± 0.02
Superior parietal cortex	ipsi	18	−82	20	4.40	337	0.16 ± 0.04	0.03 ± 0.02
Middle cingulate cortex (MCC)	contra	−14	−10	42	4.84	6886	0.15 ± 0.02	0.02 ± 0.01
Middle cingulate cortex (MCC)	ipsi	12	26	42	3.31	93	0.17 ± 0.01	0.07 ± 0.01
Superior frontal cortex	contra	−20	30	32	3.18	67	0.19 ± 0.03	0.07 ± 0.02
Superior frontal cortex	contra	−12	56	32	3.12	48	0.17 ± 0.03	0.07 ± 0.01
Superior frontal cortex	contra	−16	66	6	3.71	135	0.15 ± 0.02	0.04 ± 0.01
Anterior cingulate cortex (ACC)	contra	−12	32	28	3.45	131	0.17 ± 0.02	0.06 ± 0.01
Supramarginal gyrus	contra	−46	−36	38	3.22	60	0.17 ± 0.04	0.05 ± 0.02
Primary motor cortex (M1)	contra	−40	−6	20	3.74	84	0.13 ± 0.03	0.01 ± 0.02
Primary motor cortex (M1)	ipsi	50	6	10	3.18	124	0.13 ± 0.03	0.02 ± 0.02
Angular gyrus	contra	−26	−88	14	3.88	216	0.16 ± 0.04	0.03 ± 0.02
Angular gyrus	ipsi	48	−52	14	3.30	80	0.17 ± 0.03	0.05 ± 0.02
Angular gyrus	contra	−38	−66	8	2.97	37	0.14 ± 0.04	0.02 ± 0.02
Dorsolateral prefrontal cortex (dlPFC)	contra	−36	36	6	3.38	21	0.17 ± 0.02	0.06 ± 0.02
Dorsolateral prefrontal cortex (dlPFC)	ipsi	44	48	−2	4.00	837	0.15 ± 0.01	0.04 ± 0.01
Orbitofrontal cortex (OFC)	ipsi	22	56	−16	4.32	88	0.13 ± 0.03	0.02 ± 0.01
Piriform cortex	ipsi	20	4	−16	3.75	66	0.14 ± 0.02	0.04 ± 0.01
Piriform cortex	contra	−22	8	−24	4.15	76	0.12 ± 0.02	0.02 ± 0.01
Middle temporal gyrus	contra	−48	−8	−26	3.62	91	0.12 ± 0.02	0.03 ± 0.01
Middle temporal gyrus	ipsi	46	−4	−30	4.70	173	0.13 ± 0.02	0.04 ± 0.01

Note: All seeds are contralateral to the CRPS affected limb.

subjects with dystonia, imagined movements of the affected limb resulted in reduced IPL activation compared to control subjects (Gieteling et al., 2008). In Parkinson's disease subjects with tremor, IPL-M1 connectivity was increased compared to controls (Vervoort et al., 2016). While our study did not test the connectivity between IPL and M1, both IPL and M1 had increased connectivity to the putamen seeds contralateral to the CRPS affected limb. Thus, it is probable that increased contralateral putamen-IPL connectivity indicates dysfunction in IPL in CRPS subjects and may underlie motor dysfunction such as tremor.

Most basal ganglia seeds that displayed significant connectivity differences were motor areas; however, we also found alterations in the caudate body, which represents the striatal portion of the oculomotor loop (Alexander et al., 1986). A recent study identified this basal ganglia region as a convergence zone of corticostriatal projections with integration of reward, executive control and spatial attention during spatial reinforcement learning thought to be associated with the caudate body (Jarbo & Verstynen, 2015). In our study, the caudate body seed displayed the greatest degree of increased functional connectivity to cortical areas including M1,
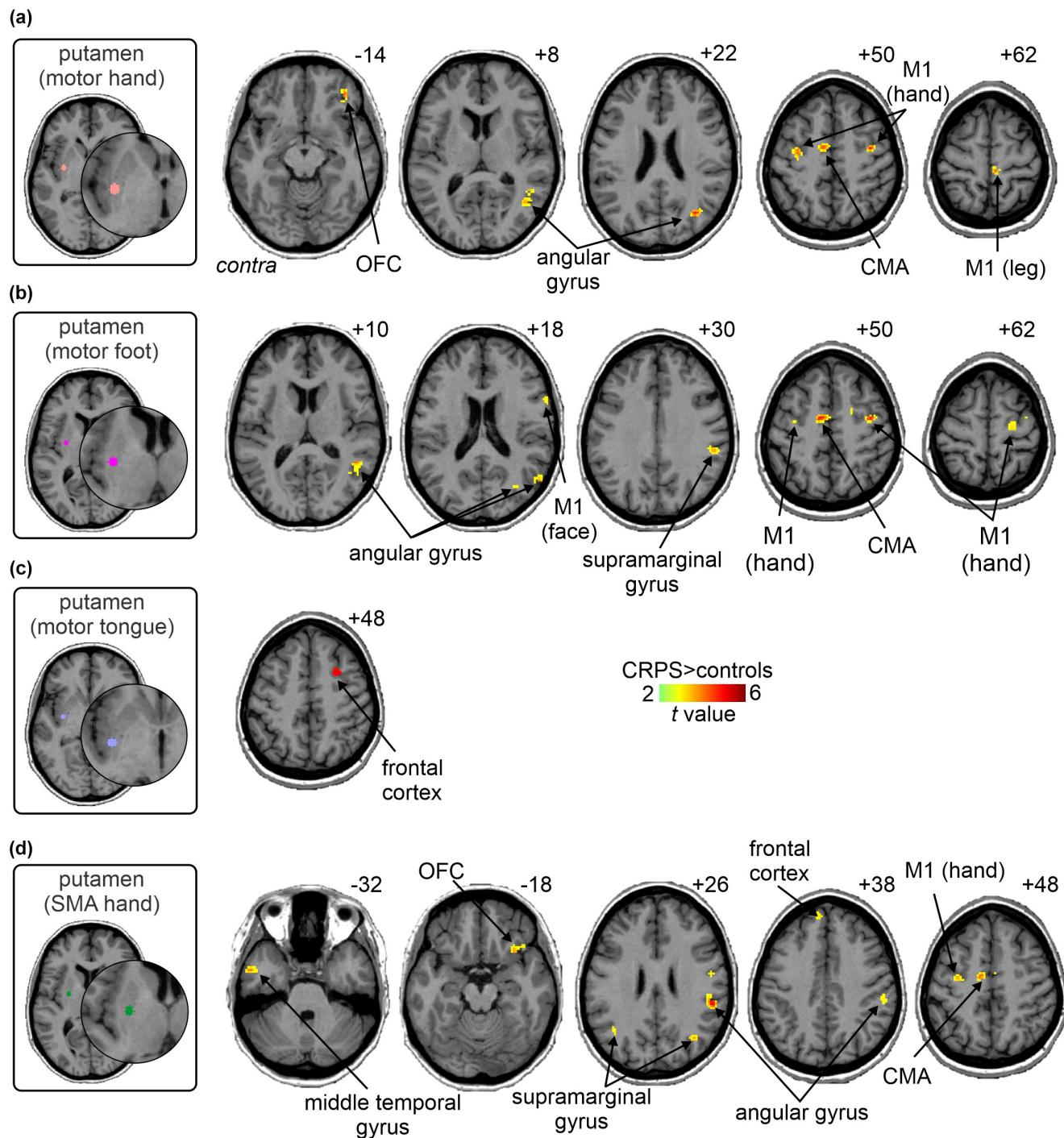
FIGURE 5 Increased functional connectivity of putamen motor loop seeds in CRPS subjects as compared with matched healthy controls. Increased functional connectivity of the putaminal (a) motor hand area, (b) motor foot area, (c) motor tongue area, and (d) the supplementary motor hand area of the putamen (SMA hand) ($p < 0.05$; false discovery rate corrected for multiple comparisons, hot color scale). Slice locations in Montreal neurological institute space are indicated on the top right of each axial slice. CMA, cingulate motor area; contra, contralateral to affected limb; M1, primary motor cortex; OFC, orbitofrontal cortex

prefrontal and parietal association cortices in CRPS subjects compared to controls. Perceptual disturbances such as neglect-like syndrome and a foreign feeling of the CRPS affected limb are common features of CRPS (Galer & Jensen, 1999; Kuttikat et al., 2016). The caudate body showed increased connectivity with cortical regions governing visual attention (middle temporal gyrus), spatial attention

(superior frontal cortex) and visuospatial perception (superior parietal cortex) and thus, may relate to the visuospatial issues in CRPS. Indeed, lesions to the caudate and the IPL can lead to deficits in visuospatial perception that present as neglect (Karnath et al., 2005; Kumral et al., 1999). However, in the current study, we did not perform correlation analysis of caudate body functional connectivity to
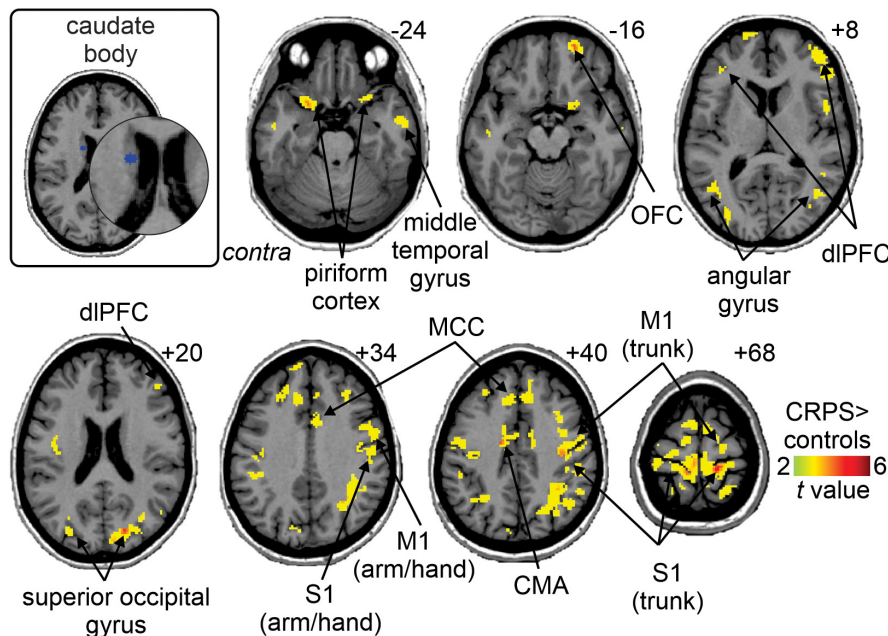
FIGURE 6 Increased functional connectivity of the caudate body seed in CRPS subjects as compared with matched healthy controls ($p < 0.05$; false discovery rate corrected for multiple comparisons, hot color scale). Slice locations in Montreal neurological institute space are indicated on the top right of each axial slice. CMA, cingulate motor area; contra, contralateral to affected limb; dlPFC, dorsolateral prefrontal cortex; M1, primary motor cortex; MCC, mid-cingulate cortex; OFC, orbitofrontal cortex; S1, primary somatosensory cortex

body perception. Thus, it is unknown to what degree visuospatial perception may be related to caudate body functional connectivity in CRPS.

There are several limitations to this study. This study had a limited sample of 15 CRPS subjects. However, given the rare nature of CRPS, it is comparable to previous studies (Di Pietro et al., 2013a, 2013b). It is noted, however, the sample size of this study is a statistically limits correlation interpretations (even when adjusted for FDR), and a much larger sample size is needed for greater reliability on correlation interpretations. The longitudinal following of subjects recruited before CRPS development would identify whether brain differences are true changes, and whether they are pathophysiological or adaptive. Furthermore, it is unknown whether the findings in our study are specific to CRPS or are also present in other pain or motor dysfunction conditions as we did not compare changes in sensory and motor disabilities between different conditions. Future studies should aim to compare changes in sensory and motor disabilities between different conditions. Nonetheless, it is clear that the sensory and motor disturbances are a result of reorganization of the sensory and motor cortices and related cortico-basal ganglia loops and are part of the CRPS disease pathology. The resting-state nature of our scanning and the lack of quantitative assessment of motor dysfunction are also weaknesses. Future studies should include quantitative assessment of motor dysfunction (e.g., pegboard task, Unified Parkinson Disease Rating Scale) or examine functional connectivity during movement tasks (e.g., finger tapping, wrist extension)—although this would present a practical challenge. Medications

may have had a potential effect on results as 13 of the 15 CRPS subjects had taken medication before the study; however, it is not easy or necessarily ethical to exclude medicated CRPS subjects or include a washout period before the study. Ideally, the study would have recruited CRPS participants with no comorbidities, however, given the rare nature of CRPS and multi-system dysfunction following CRPS (Schwartzman, 2012), this was difficult. Hence, it cannot be fully excluded that multiple comorbidities may have also had a potential effect in this study's findings. However, all CRPS participants had been diagnosed with CRPS, and the list of comorbidities varies greatly between each CRPS participant. Given the great variability, collectively the multiple comorbidities are unlikely to contribute significantly to the overall changes reported in this study.

5 | CONCLUSION

Our study is the first to systematically evaluate infraslow oscillations and resting-state functional connectivity in motor and non-motor basal ganglia functional loops in CRPS subjects. Compared to controls, we identified increased ISOs in the putamen contralateral to the CRPS affected side, but not in non-motor basal ganglia regions in CRPS subjects. Moreover, putaminal ISOs correlated with wrist function and disability scores. We demonstrated increased functional connectivity in the contralateral putamen (especially the motor hand region) and caudate body seeds, with a network of cortical structures including the M1 hand region, SMA, and other frontal

and parietal association cortices. There were no changes in striatal seeds representing cognitive and limbic basal ganglia loops. In summary, the recruitment of anatomically specific motor basal ganglia-cortical networks likely underlies motor symptoms, such as dystonia and tremor, while the caudate body network may be related to altered visuospatial integration, in CRPS.

CONFLICT OF INTEREST

The authors have no conflict of interest to declare.

AUTHOR CONTRIBUTIONS

All authors had full access to all the data in the study and take responsibility for the integrity of the data and the accuracy of the data analysis. *Conceptualization*, F.D.P., L.A.H., and P.J.A.; *Methodology*, F.D.P., L.A.H., and P.J.A.; *Investigation*, B.L. and F.D.P.; *Formal Analysis*, B.L., L.A.H., and P.J.A.; *Writing – Original Draft*, B.L., L.A.H., and P.J.A.; *Writing – Review & Editing*, B.L., F.D.P., L.A.H., and P.J.A.; *Visualization*, B.L., F.D.P., L.A.H., and P.J.A.; *Supervision*, F.D.P., L.A.H., and P.J.A.; *Funding Acquisition*, F.D.P.

PEER REVIEW

The peer review history for this article is available at https://publons.com/publon/10.1002/jnr.25057.

DATA AVAILABILITY STATEMENT

Data sharing not available due to privacy/ethical restrictions.

ORCID

Barbara Lee https://orcid.org/0000-0001-9665-660X
Paul J. Austin https://orcid.org/0000-0001-5253-6876

REFERENCES

Agulhon, C., Boyt, K. M., Xie, A. X., Friocourt, F., Roth, B. L., & Mccarthy, K. D. (2013). Modulation of the autonomic nervous system and behaviour by acute glial cell Gq protein-coupled receptor activation in vivo. *Journal of Physiology*, *591*(22), 5599–5609.

Al-Amin, H., Sarkis, R., Atweh, S., Jabbur, S. & Saadé, N. (2011). Chronic dizocilpine or apomorphine and development of neuropathy in two animal models II: Effects on brain cytokines and neurotrophins. *Experimental Neurology*, *228*(1), 30–40.

Albin, R. L., Young, A. B., & Penney, J. B. (1989). The functional anatomy of basal ganglia disorders. *Trends in Neurosciences*, *12*(10), 366–375.

Alexander, G. E., Delong, M. R., & Strick, P. L. (1986). Parallel organization of functionally segregated circuits linking basal ganglia and cortex. *Annual Review of Neuroscience*, *9*, 357–381.

Alshelh, Z., Di Pietro, F., Youssef, A. M., Reeves, J. M., Macey, P. M., Vickers, E. R., Peck, C. C., Murray, G. M., & Henderson, L. A. (2016). Chronic neuropathic pain: It's about the rhythm. *Journal of Neuroscience*, *36*(3), 1008.

Apkarian, A. V., Lavarello, S., Randolf, A., Berra, H. H., Chialvo, D. R., Besedovsky, H. O., & Del Rey, A. (2006). Expression of IL-1β in supraspinal brain regions in rats with neuropathic pain. *Neuroscience Letters*, *407*(2), 176–181.

Azqueta-Gavaldon, M., Youssef, A. M., Storz, C., Lemme, J., Schulte-Göcking, H., Becerra, L., Azad, S. C., Reiners, A., Ertl-Wagner, B., Borsook, D., Upadhyay, J., & Kraft, E. (2020). Implications of the putamen in pain and motor deficits in complex regional pain syndrome. *Pain*, *161*(3), 595–608.

Bean, D. J., Johnson, M. H., & Kydd, R. R. (2014). The outcome of complex regional pain syndrome type 1: A systematic review. *Journal of Pain*, *15*(7), 677–690.

Beaton, D. E., Wright, J. G., Katz, J. N., & Upper Extremity Collaborative Group. (2005). Development of the QuickDASH: Comparison of three item-reduction approaches. *Journal of Bone and Joint Surgery*, *87*(5), 1038–1046.

Becerra, L., Sava, S., Simons, L. E., Drosos, A. M., Sethna, N., Berde, C., Lebel, A. A., & Borsook, D. (2014). Intrinsic brain networks normalize with treatment in pediatric complex regional pain syndrome. *Neuroimage Clinical*, *6*, 347–369.

Benjamini, Y., & Hochberg, Y. (1995). Controlling the false discovery rate: A practical and powerful approach to multiple testing. *Journal of the Royal Statistical Society: Series B (Methodological)*, *57*(1), 289–300.

Borsook, D., Upadhyay, J., Chudler, E. H., & Becerra, L. (2010). A key role of the basal ganglia in pain and analgesia—Insights gained through human functional imaging. *Molecular Pain*, *6*, 27.

Buzsaki, G., & Draguhn, A. (2004). Neuronal oscillations in cortical networks. *Science*, *304*(5679), 1926–1929.

Caspers, S., Schleicher, A., Bacha-Trams, M., Palomero-Gallagher, N., Amunts, K., & Zilles, K. (2013). Organization of the human inferior parietal lobule based on receptor architectonics. *Cerebral Cortex*, *23*(3), 615–628.

Chao-Gan, Y., & Yu-Feng, Z. (2010). DPARSF: A MATLAB toolbox for "pipeline" data analysis of resting-state fMRI. *Frontiers in Systems Neuroscience*, *4*, 13.

Choi, E. Y., Yeo, B. T. T., & Buckner, R. L. (2012). The organization of the human striatum estimated by intrinsic functional connectivity. *Journal of Neurophysiology*, *108*(8), 2242–2263.

Cornell-Bell, A. H., Finkbeiner, S. M., Cooper, M. S., & Smith, S. J. (1990). Glutamate induces calcium waves in cultured astrocytes: Long-range glial signaling. *Science*, *247*(4941), 470.

Crunelli, V., Blethyn, K. L., Cope, D. W., Hughes, S. W., Parri, H. R., Turner, J. P., Tòth, T. I., & Williams, S. R. (2002). Novel neuronal and astrocytic mechanisms in thalamocortical loop dynamics. *Philosophical Transactions of the Royal Society of London: Series B, Biological Sciences*, *357*(1428), 1675–1693.

Da Cunha, C., Gomez, A., & Blaha, C. D. (2012). The role of the basal ganglia in motivated behavior. *Reviews in the Neurosciences*, *23*(5–6), 747–767.

Del Valle, L., Schwartzman, R. J., & Alexander, G. (2009). Spinal cord histopathological alterations in a patient with longstanding complex regional pain syndrome. *Brain, Behavior, and Immunity*, *23*(1), 85–91.

Di Pietro, F., Lee, B., & Henderson, L. A. (2020). Altered resting activity patterns and connectivity in individuals with complex regional pain syndrome. *Human Brain Mapping*, *41*(13), 3781–3793.

Di Pietro, F., Mcauley, J. H., Parkitny, L., Lotze, M., Wand, B. M., Moseley, G. L., & Stanton, T. R. (2013a). Primary motor cortex function in complex regional pain syndrome: A systematic review and meta-analysis. *Journal of Pain*, *14*(11), 1270–1288.

Di Pietro, F., Mcauley, J. H., Parkitny, L., Lotze, M., Wand, B. M., Moseley, G. L., & Stanton, T. R. (2013b). Primary somatosensory cortex function in complex regional pain syndrome: A systematic review and meta-analysis. *Journal of Pain*, *14*(10), 1001–1018.

Fiore, N. T., & Austin, P. J. (2016). Are the emergence of affective disturbances in neuropathic pain states contingent on supraspinal neuroinflammation? *Brain, Behavior, and Immunity*, *56*, 397–411.

Friston, K. J., Holmes, A. P., Worsley, K. J., Poline, J. P., Frith, C. D., & Frackowiak, R. S. (1995). Statistical parametric maps in functional imaging: A general linear approach. *Human Brain Mapping*, *2*(4), 189–210.

Galer, B. S., & Jensen, M. (1999). Neglect-like symptoms in complex regional pain syndrome. *Journal of Pain and Symptom Management*, *18*(3), 213–217.

Geha, P. Y., Baliki, M. N., Harden, R. N., Bauer, W. R., Parrish, T. B., & Apkarian, A. V. (2008). The brain in chronic CRPS pain: Abnormal gray-white matter interactions in emotional and autonomic regions. *Neuron*, *60*(4), 570–581.

Gerke, M. B., Duggan, A. W., Xu, L., & Siddall, P. J. (2003). Thalamic neuronal activity in rats with mechanical allodynia following contusive spinal cord injury. *Neuroscience*, *117*(3), 715–722.

Gieteling, E. W., Van Rijn, M. A., De Jong, B. M., Hoogduin, J. M., Renken, R., Van Hilten, J. J., & Leenders, K. L. (2008). Cerebral activation during motor imagery in complex regional pain syndrome type 1 with dystonia. *Pain*, *134*(3), 302–309.

Harden, R. N., Bruehl, S., Stanton-Hicks, M., & Wilson, P. R. (2007). Proposed new diagnostic criteria for complex regional pain syndrome. *Pain Medicine*, *8*(4), 326–331.

Henderson, L., & Di Pietro, F. (2016). How do neuroanatomical changes in individuals with chronic pain result in the constant perception of pain? *Pain Management*, *6*, 147–159.

Hotta, J., Saari, J., Koskinen, M., Hlushchuk, Y., Forss, N., & Hari, R. (2017). Abnormal brain responses to action observation in complex regional pain syndrome. *Journal of Pain*, *18*(3), 255–265.

Hou, Y., Wu, X., Hallett, M., Chan, P., & Wu, T. (2014). Frequency-dependent neural activity in Parkinson's disease. *Human Brain Mapping*, *35*(12), 5815–5833. https://doi.org/10.1002/hbm.22587

Iwata, M., Leblanc, B. W., Kadasi, L. M., Zerah, M. L., Cosgrove, R. G., & Saab, C. Y. (2011). High-frequency stimulation in the ventral posterolateral thalamus reverses electrophysiologic changes and hyperalgesia in a rat model of peripheral neuropathic pain. *Pain*, *152*(11), 2505–2513.

Jarbo, K., & Verstynen, T. D. (2015). Converging structural and functional connectivity of orbitofrontal, dorsolateral prefrontal, and posterior parietal cortex in the human striatum. *Journal of Neuroscience*, *35*(9), 3865–3878.

Jeon, S. Y., Seo, S., Lee, J. S., Choi, S.-H., Lee, D.-H., Jung, Y.-H., Song, M.-K., Lee, K.-J., Kim, Y. C., Kwon, H. W., Im, H.-J., Lee, D. S., Cheon, G. J., & Kang, D.-H. (2017). [11C]-(R)-PK11195 positron emission tomography in patients with complex regional pain syndrome: A pilot study. *Medicine*, *96*(1), e5735.

Karnath, H. O., Zopf, R., Johannsen, L., Fruhmann Berger, M., Nägele, T., & Klose, U. (2005). Normalized perfusion MRI to identify common areas of dysfunction: Patients with basal ganglia neglect. *Brain*, *128*(Pt 10), 2462–2469.

Kumral, E., Evyapan, D., & Balkir, K. (1999). Acute caudate vascular lesions. *Stroke*, *30*(1), 100–108.

Kuttikat, A., Noreika, V., Shenker, N., Chennu, S., Bekinschtein, T., & Brown, C. A. (2016). Neurocognitive and neuroplastic mechanisms of novel clinical signs in CRPS. *Frontiers in Human Neuroscience*, *10*, 16.

Lebel, A., Becerra, L., Wallin, D., Moulton, E. A., Morris, S., Pendse, G., Jasciewicz, J., Stein, M., Aiello-Lammens, M., Grant, E., Berde, C., & Borsook, D. (2008). fMRI reveals distinct CNS processing during symptomatic and recovered complex regional pain syndrome in children. *Brain*, *131*(7), 1854–1879.

Lee, B., Henderson, L. A., Rae, C. D., & Di Pietro, F. (2020). CRPS is not associated with altered sensorimotor cortex GABA or glutamate. *eNeuro*, *7*(1), ENEURO.0389-19.2020.

Lewis, J. S., & McCabe, C. S. (2010). Body perception disturbance (BPD) in CRPS. *Practical Pain Management*, *10*, 60–66.

Linnman, C., Becerra, L., Lebel, A., Berde, C., Grant, P. E., & Borsook, D. (2013). Transient and persistent pain induced connectivity alterations in pediatric complex regional pain syndrome. *PLoS ONE*, *8*(3), e57205.

MacDermid, J. C. (1996). Development of a scale for patient rating of wrist pain and disability. *Journal of Hand Therapy*, *9*(2), 178–183.

Macey, P. M., Macey, K. E., Kumar, R., & Harper, R. M. (2004). A method for removal of global effects from fMRI time series. *Neuroimage*, *22*(1), 360–366. https://doi.org/10.1016/j.neuroimage.2003.12.042.

Maihöfner, C., Baron, R., Decol, R., Binder, A., Birklein, F., Deuschl, G., Handwerker, H. O., & Schattschneider, J. (2007). The motor system shows adaptive changes in complex regional pain syndrome. *Brain*, *130*(10), 2671–2687.

Marinus, J., Moseley, G. L., Birklein, F., Baron, R., Maihöfner, C., Kingery, W. S., & Van Hilten, J. J. (2011). Clinical features and pathophysiology of complex regional pain syndrome. *Lancet Neurology*, *10*(7), 637–648.

Middleton, F. A., & Strick, P. L. (1996). The temporal lobe is a target of output from the basal ganglia. *Proceedings of the National Academy of Sciences of the United States of America*, *93*(16), 8683.

Nambu, A., Kaneda, K., Tokuno, H., & Takada, M. (2002). Organization of corticostriatal motor inputs in monkey putamen. *Journal of Neurophysiology*, *88*(4), 1830–1842.

Neychev, V. K., Gross, R. E., Lehéricy, S., Hess, E. J., & Jinnah, H. A. (2011). The functional neuroanatomy of dystonia. *Neurobiology of Disease*, *42*(2), 185–201.

Okada-Ogawa, A., Suzuki, I., Sessle, B. J., Chiang, C.-Y., Salter, M. W., Dostrovsky, J. O., Tsuboi, Y., Kondo, M., Kitagawa, J., Kobayashi, A., Noma, N., Imamura, Y., & Iwata, K. (2009). Astroglia in medullary dorsal horn (trigeminal spinal subnucleus caudalis) are involved in trigeminal neuropathic pain mechanisms. *Journal of Neuroscience*, *29*(36), 11161.

Opri, E., Cernera, S., Okun, M. S., Foote, K. D., & Gunduz, A. (2019). The functional role of thalamocortical coupling in the human motor network. *Journal of Neuroscience*, *39*(41), 8124.

Padmashri, R., Suresh, A., Boska, M. D., & Dunaevsky, A. (2015). Motor-skill learning is dependent on astrocytic activity. *Neural Plasticity*, *2015*, 938023.

Redgrave, P., Rodriguez, M., Smith, Y., Rodriguez-Oroz, M. C., Lehericy, S., Bergman, H., Agid, Y., Delong, M. R., & Obeso, J. A. (2010). Goal-directed and habitual control in the basal ganglia: Implications for Parkinson's disease. *Nature Reviews Neuroscience*, *11*(11), 760–772.

Redgrave, P., Vautrelle, N., & Reynolds, J. N. J. (2011). Functional properties of the basal ganglia's re-entrant loop architecture: Selection and reinforcement. *Neuroscience*, *198*, 138–151.

Rolls, E. T., Cheng, W., & Feng, J. (2020). The orbitofrontal cortex: Reward, emotion and depression. *Brain Communications*, *2*(2), fcaa196.

Särkkä, S., Solin, A., Nummenmaa, A., Vehtari, A., Auranen, T., Vanni, S., & Lin, F.-H. (2012). Dynamic retrospective filtering of physiological noise in BOLD fMRI: DRIFTER. *NeuroImage*, *60*(2), 1517–1527.

Sarnthein, J., Stern, J., Aufenberg, C., Rousson, V., & Jeanmonod, D. (2006). Increased EEG power and slowed dominant frequency in patients with neurogenic pain. *Brain*, *129*(Pt 1), 55–64.

Schwartzman, R. (2012). Systemic complications of complex regional pain syndrome. *Neuroscience & Medicine*, *3*, 225–242.

Schwenkreis, P., Maier, C., & Tegenthoff, M. (2009). Functional imaging of central nervous system involvement in complex regional pain syndrome. *American Journal of Neuroradiology*, *30*(7), 1279–1284.

Seo, S., Jung, Y.-H., Lee, D., Lee, W. J., Jang, J. H., Lee, J.-Y., Choi, S.-H., Moon, J. Y., Lee, J. S., Cheon, G. J., & Kang, D.-H. (2021). Abnormal

neuroinflammation in fibromyalgia and CRPS using [11C]-(R)-PK11195 PET. *PLoS ONE, 16*(2), e0246152.

Simioni, A. C., Dagher, A., & Fellows, L. K. (2015). Compensatory striatal-cerebellar connectivity in mild-moderate Parkinson's disease. *Neuroimage Clinical, 10*, 54–62.

Starr, C. J., Sawaki, L., Wittenberg, G. F., Burdette, J. H., Oshiro, Y., Quevedo, A. S., Mchaffie, J. G., & Coghill, R. C. (2011). The contribution of the putamen to sensory aspects of pain: Insights from structural connectivity and brain lesions. *Brain, 134*(7), 1987–2004.

Vanneste, S., Song, J.-J., & De Ridder, D. (2018). Thalamocortical dysrhythmia detected by machine learning. *Nature Communications, 9*(1), 1103.

Vervoort, G., Alaerts, K., Bengevoord, A., Nackaerts, E., Heremans, E., Vandenberghe, W., & Nieuwboer, A. (2016). Functional connectivity alterations in the motor and fronto-parietal network relate to behavioral heterogeneity in Parkinson's disease. *Parkinsonism & Related Disorders, 24*, 48–55.

Wang, Z., Liu, Y., Ruan, X., Li, Y., Li, E., Zhang, G., Li, M., & Wei, X. (2020). Aberrant amplitude of low-frequency fluctuations in different frequency bands in patients with Parkinson's disease. *Frontiers in Aging Neuroscience, 12*, 576682. https://doi.org/10.3389/fnagi.2020.576682

SUPPORTING INFORMATION

Additional supporting information may be found in the online version of the article at the publisher's website.

FIGURE S1 One-sample *t*-test within group results for putamen seeds; a: putamen ISO, b: putamen (motor hand), c: putamen (motor foot), d: putamen (motor tongue), and e putamen (SMA hand). Figures were masked using frontal lobe, anterior cingulate cortex (ACC), middle temporal gyrus and parietal lobe and visualised at a threshold of *p* = 0.05 FDR and 20 voxel minimum cluster size

FIGURE S2 One-sample *t*-test within group results for non-motor basal ganglia seeds; a: caudate body, b: caudate tail, c: ventrolateral (vl) caudate head, d: dorsolateral (dl) caudate head, e: ventral striatum, and f: ventral putamen. Figures were masked using frontal lobe, anterior cingulate cortex (ACC), middle temporal gyrus and parietal lobe and visualised at a threshold of *p* = 0.05 FDR and 20 voxel minimum cluster size. The ventral striatum CRPS (e) did not have any contrast at *p* = 0.05 FDR, 20 voxel minimum cluster size when masked with the frontal lobe, anterior cingulate cortex (ACC), middle temporal gyrus and parietal lobe mask